Development and Testing of Electrical Joints for the 36-T Series-Connected Hybrid Magnet

Ting Xu, Tom A. Painter, Hubertus W. Weijers, Todd Adkins, Scott Bole, Yehia M. Eyssa, Jun Lu, John R. Miller, George E. Miller, and Patrick D. Noyes

***Abstract*—Here, we report the development of the CICC joint design for the 36-T Series-Connected Hybrid Magnet. A novel solder-less single-box praying-hands joint has been designed to meet the mission of the SCH. A prototype sample joint, Florida Solder-less Joint A (FSJ-A), was manufactured and tested. The low DC resistance confirmed the feasibility of the concept design. In addition, a simple model describing the current transient behavior of the pray-hand joint is presented. A comparison with the experimental data is also included.**

***Index Terms*—Nb_3Sn CICC, praying-hands joint, series-connected-hybrid-magnet, superconducting magnet.**

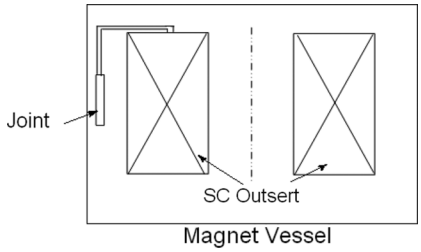

Fig. 1. Schematic of joint layout.

I. Introduction

THE design of the 36-T Series-Connected-Hybrid Magnet (SCH) for the National High Magnetic Field Laboratory (NHMFL) includes a resistive insert and a superconducting outsert [1]. The superconducting outsert itself consists of three concentric layer-wound subcoils using different grades Nb_3Sn Cable-in-Conduit-Conductors. The splices and terminals of the subcoils are designed to be placed outside the 36-T SCH (approximately 0.75 m in radius) and aligned with the magnetic axial field as shown in Fig. 1. The joints are in praying-hands configuration. Low magnetic field and favorable orientation minimize the AC losses in the joints during magnet ramp and discharge. The cryogenic budget for each joint at normal running mode is 0.8 W, which requires the joint DC resistance to be less than 2 $n\Omega$.

Here, we report the concept design of a novel solder-less joint for the 36-T SCH and the manufacture and testing of the first prototype joint sample using 45-T coil-A cable [2]. A quantitative comparison of the current transient with solder-filled praying-hands joint is also presented.

II. Joint Design and Fabrication

A. Concept Design

The design philosophy of the 36-T SCH joints is simple, robust and well balanced between DC resistance and AC losses according to its mission. Following this guideline, we designed and manufactured the first sample joint based on the Florida Solder-less Joint Technology (patent pending). The joint is enclosed in a stainless steel joint box entirely as shown in Fig. 2. The configuration provides a long term worry free vacuum tightness and voids the bond between thermal mismatch materials like copper and stainless steel, which may lead joint deformation during heat treatment as reported by D.Ciazynski *et al.* [3]. The superconducting cables are compressed in the joint assembly against the OFHC copper plate at the middle using the tooling shown in Fig. 2(c). The final void fraction is designed to be 20%. The strands and the copper plate are sintered together during the first stage of the heat treatment, which provides a good current transfer without bearing a large penalty in AC losses. This eliminates the need for solder filling and other post-heat treatment processing, which reduces the risk of damage to the expensive superconductor in the brittle state. However, the single box design also means the joint can not be disassembled afterwards, which may limit it to be used for the applications that dismountable joints are required. Two cooling channels are designed to be machined on both sides of the winged copper plate to enhance the cooling inside the joint, which is not implanted to this initial test, but will be provided in the final joint assembly.

B. Fabrication of Joint Sample FSJ-A

1) Cable preparation
   - Remove conduit jacket to expose proper length cable
   - Remove stainless foil and wrap a steel wire around the cable approximately every 25 mm to prevent untwisting.
2) Etch off the chrome plate on the strands using 37% hydrochloric acid. The process is not applied to the current joint, since 45-T A cable strands are not plated.
3) Clean all the cables with isopropyl alcohol.
4) Assemble joint parts and cables together in the order of: bottom plate $\Rightarrow$ bottom cable $\Rightarrow$ copper plate $\Rightarrow$ upper cable $\Rightarrow$ lid as shown in Fig. 2(a).

Manuscript received August 16, 2008. First published June 23, 2009; current version published July 15, 2009. This work was supported in part by the U.S. National Science Foundation under Grant DMR-0603042 and Helmholtz Center Berlin.

T. Xu, T. A. Painter, H. W. Weijiers, T. Adkins, S. Bole, J. Lu, G. E. Miller, and P. D. Noyes are with the National High Magnetic Field Laboratory, Tallahassee, FL 32310 USA (e-mail: tingxu@magnet.fsu.edu).

Y. M. Eyssa was with the National High Magnetic Field Laboratory, Tallahassee, FL 32310, USA. He is now retired.

J. R. Miller is with US-ITER, Oak Ridge National Laboratory, TN USA.

Color versions of one or more of the figures in this paper are available online at http://ieeexplore.ieee.org.

Digital Object Identifier 10.1109/TASC.2009.2019224

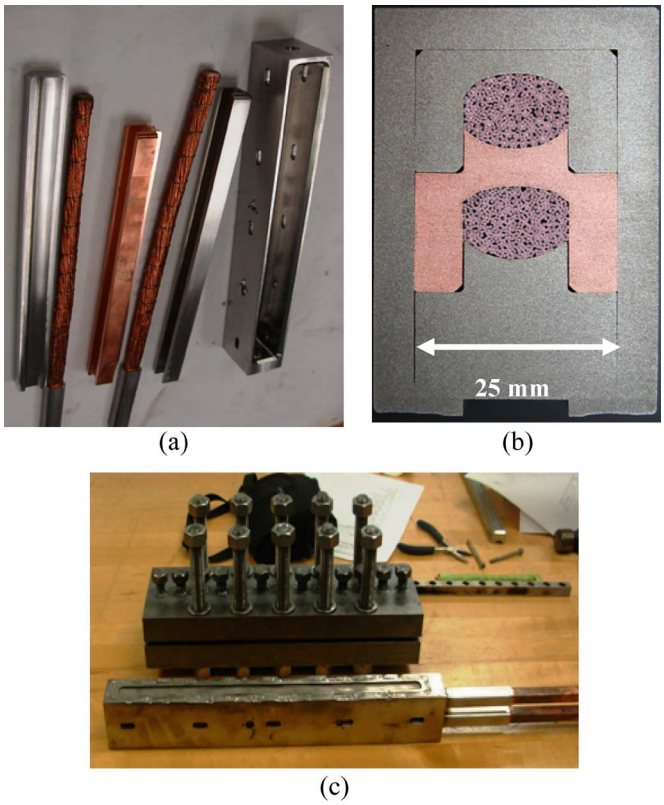

Fig. 2. FSJ-A sample joint. (a) FSJ-A joint parts; (b) joint cross-section view; (c) joint compress tooling.

5) Compress
   - Place the joint assembly into the compress tooling as shown in Fig. 2(c)
   - Compress the cable inside the joint box by tightening down the bolts in the center line of the tooling. Use torque wrench to achieve equal pressure along the joint length.
   - Spot weld along the lid at several places after final voids achieved.
6) TIG weld the lid entirely to seal the joint box.
7) Heat treat the joint as follows
   100 hrs @ 210°C
   48 hrs @ 340°C
   60 hrs @ 625°C
   with a 50°C/h ramp rate for all steps.

Fig. 2(b) shows the cross-section of the FSJ-A after heat treatment.

III. Experimental Setup

Shown in Fig. 3 is the experimental rig of the DC resistance measurement. The sample joint is immersed in saturated He I bath at 4.2 K during the experiment. The current is supplied by a 20 kA DC power supply through the vapor cooled current leads. Two different methods have been used to measure the joint resistance. First, we obtained the joint resistance by measuring the voltage drop across the joint V_1, in steady state with known transport current values. In addition to this, we can also obtain the joint resistance by measuring the current diffusion in the joints during ramping. The transient current distribution in the joint along the longitudinal direction z can be written as,

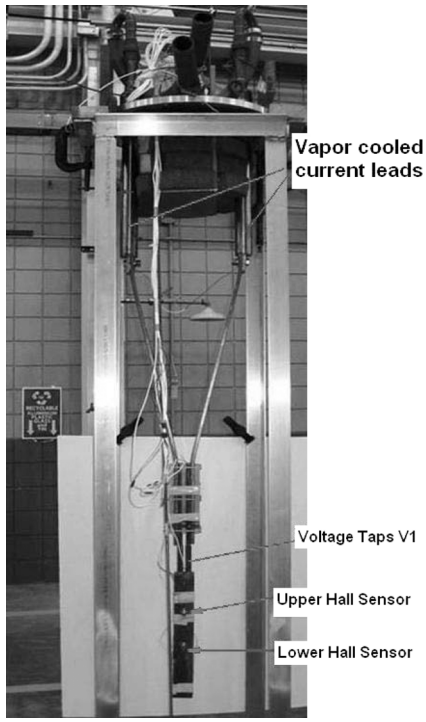

Fig. 3. Experimental setup for the joint test.

$$\frac{\partial^2 I}{\partial z^2} = \frac{L/Z_0}{RZ_0}\frac{\partial I}{\partial t} = \frac{\tau_0}{Z_0^2}\frac{\partial I}{\partial t} \tag{1}$$

where L is the inductance of the joint, R is the resistance of the joint, Z_0 is the total current transfer length, and $\tau_0 = L/R$. By assuming the homogenous current distribution within the cable, we can express the specific inductance L/Z_0 as [4],

$$\frac{L}{Z_0} = \frac{\mu_0}{\pi}\left[\ln\left(\frac{a}{d/2 - \sqrt{d^2/4 - a^2}}\right) + \frac{1}{4}\right] \tag{2}$$

where a is the radius of the cable and d is the distance between the two cable centers. For the current joint geometry, this gives $L \approx 0.15\ \mu\mathrm{H}$. Therefore, the diffusion time will be on the order of 10^2 seconds according to the expected nano-Ohm joint resistance and quite sensitive to the actual value of it.

In order to capture the current transient along the joint length, two hall sensors are placed at one third and two thirds of the lapping length respectively as shown in Fig. 3. The sensing elements are centered transversely over the copper section between the cables so that they were in the best orientation to measure the self field generated by the transport current.

IV. Results and Discussion

The joint resistance obtained by the voltage measurement is generally less than 1.7 $\mathrm{n}\Omega$ with a transport current up to 19.5 kA as the solid square shown in Fig. 4. One interesting aspect in this result is that the joint resistance shows a quite strong dependence on the transport current. This current dependency can not be explained by the magneto-resistivity raise of the copper in

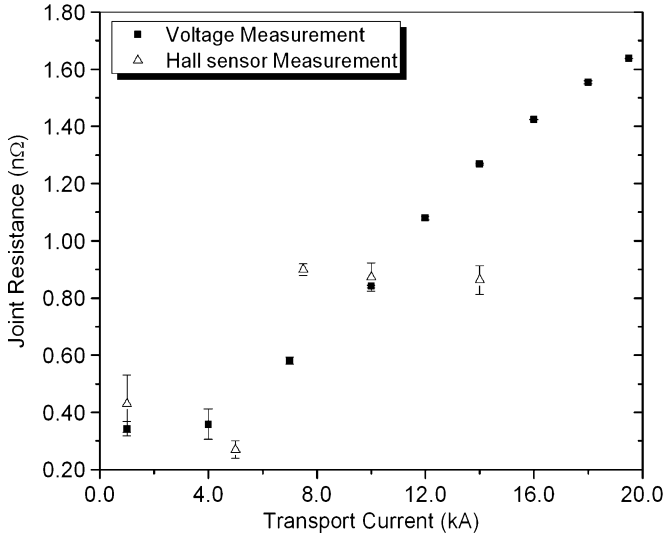

Fig. 4. Measured joint resistance of FSJ-A as a function of the transport current.

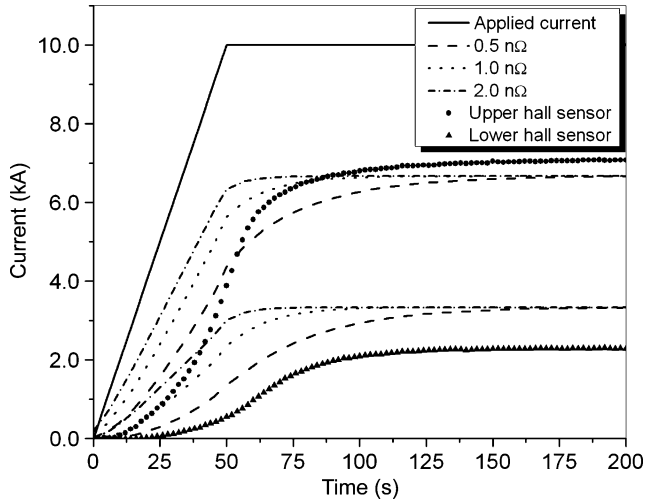

Fig. 5. The current variation as a function of time at two different locations along the FSJ-A sample joint for the case of a linear ramp at 200 A/s and hold steady at 10 kA afterwards.

the joint from the increased self-field, which would only explain about 0.05 nΩ from 0 to 19.5 kA. In order to put further discussion on this observation, it is helpful to show the hall sensor measurements first.

Fig. 5 shows the current measurements by the Hall sensors for a linear 200 A/s ramp to 10 kA followed by a hold for 400 seconds to allow the current diffusion in the joint to reach equilibrium state. In the figure, the solid circle and solid triangle are the measurements obtained from the upper and lower hall sensors, respectively. The dash, dot and short dash dot lines are the calculations using (1) for different joint resistance R with the boundary conditions that $I|_{z=0} = I(t)$, and $I|_{z=Z_0} = 0$. In this case, (1) has an analytic solution, which can be expressed as,

$$I(z,\tau)=\frac{I_{\max}}{\tau_1}\left(\left(1-\frac{z}{Z_0}\right)\tau-\frac{2Z_0^2}{\pi^3}\times\sum_{n=1}^{\infty}\sin\left(\frac{n\pi z}{Z_0}\right)\frac{1-e^{\frac{-n^2\pi^2\tau}{Z_0^2}}}{n^3}\right)\quad(t<t_1),$$

$$I(z,\tau)=I_{\max}\left[\left(1-\frac{z}{Z_0}\right)-\frac{2}{\pi}\left(1-\frac{\tau_1}{\tau_o}\right)\times\sum_{n=1}^{\infty}\sin\left(\frac{n\pi z}{Z_0}\right)e^{\frac{-n^2\pi^2(\tau-\tau_1)}{Z_0^2}}\right]-\frac{I_{\max}}{\tau_o}\frac{2Z_0^2}{\pi^3}\sum_{n=1}^{\infty}\frac{1}{n^3}\sin\left(\frac{n\pi z}{Z_0}\right)\times\left[e^{\frac{-n^2\pi^2(\tau-\tau_1)}{Z_0^2}}-e^{\frac{-n^2\pi^2\tau}{Z_0^2}}\right]\quad(t>t_1),\qquad(3)$$

where t_1 is the ramping time, $\tau = t/\tau_0$ and $\tau_1 = t_1/\tau_0$. The result shows that at 10 kA the current transferring through the lower portion of the joint is much lower than the predicted linear distribution in the calculation. In order to convert the result to the resistance of the joint, we normalize the data to their steady state values. We calculate the time interval taken the current to reach 95% of their steady state values and compared with the calculation using (3) to get the resistance value. The results are showed

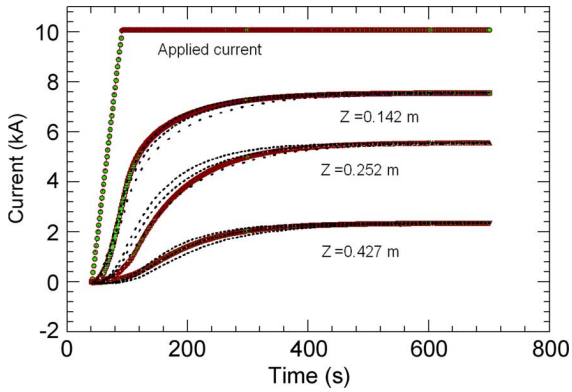

Fig. 6. The current variation as a function of time at three different locations along the 45-T solder-filled praying-hands joint for the case of a linear ramp at 200 A/s and hold steady at 10 kA afterwards. The dot lines are the calculations using (3) with three different joint resistances: 0.38 nΩ, 0.32 nΩ and 0.27 nΩ respectively. The lapping length of the joint Z_0 is 0.56 m, cable radius a is 7.1 mm, and distance between the cable d is 22.6 mm.

in Fig. 1 as hollow triangles. The data are in the same order of magnitude as the DC voltage measurements. Fig. 6 shows the similar measurements done in previously unreported work for the praying-hands solder-filled joint using the same 45-T coil-A cable. The current is linearly distributed along the 0.56 m length in this case, which indicates that the current is equally transferred along the lapping length for solder-filled joint. This makes us speculate that the uneven current distribution may be caused by the relatively high contact resistance in the joint.

Here, we plot the dimensionless current distribution along the solder-less joint vs the total transport current I_{max} in Fig. 7. The portion of the total current transferred by the lower part of the joint increases with the transport current up to 12 kA. The driving force of this change in current distribution is voltage. This explains why we saw a strong current dependent joint resistance in voltage measurements. The reason causes this is not clear to us yet. One possible explanation of this change is that with the current increase more and more stands start to carry current as the strands contacted with the copper plate become

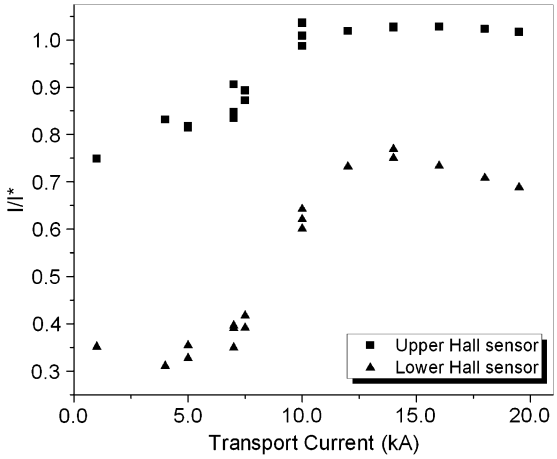

Fig. 7. Current distribution along the joint length as a function of the transport current. I^* is the calculated value for the steady state using (3) and I is the measured steady state value.

saturated in the joint self-field. The relative higher contact resistances between strands contribute to the voltage drop increase in addition to the resistance of the copper plate between the cables as the current has to be transferred between strands. We expect that improving the sinter between the strands will help to reduce this effect.

V. Summary

The concept joint design for the SCH has been finished. A prototype joint sample FSJ-A has been fabricated and tested in the National High Magnetic Field Laboratory. The results show that the DC resistance of the FSJ-A is below the maximum allowed design value (2.0 $\mathrm{n\Omega}$ at 20 kA. The joint shows a non-linear current transport along the lapping length, which is not observed in the same configuration solder-filled joint. Further effort to improve the copper sinter in the heat treatment is on going. Manufacture of another joint sample FSJ-B using the full size SCH cable to be tested in magnetic field is on schedule. The test will be focus on measuring AC losses and examining the load cycle effect on the joint performance.

References

[1] A. B. Oliva *et al.*, "Development of the superconducting outserts for the series-connected-hybrid program at the National High Magnetic Field Laboratory," *IEEE Trans. Appl. Supercond.*, vol. 18, no. 2, pp. 529–535, Jun. 2008.

[2] T. A. Painter, "Progress in the manufacture of the cable-in-conduit $\mathrm{Nb_3Sn}$ outsert coils for the 45 T Tesla hybrid Magnet," *IEEE Trans. Magn.*, vol. 30, no. 4, pp. 2204–2207, Jul. 1994.

[3] D. Ciazynski, "Fabrication of the first European full-size joint sample for ITER," *IEEE Trans. Appl. Supercond.*, vol. 9, no. 2, pp. 648–651, Jun. 1999.

[4] H. Hnoepfel, *Pulsed High Magnetic Fields*. : North-Holland Publishing Co, 1970, pp. 35–36.